Supplementary Information

Ligand Modification on Organotin-Oxo Clusters for Enhanced Third-Order Nonlinear Optical Response

Yang-Hong Liu,[a,b,c] Hao Li, [a,b,c] Hui-Ru Lou,[a,b,c] Er-Xia, Chen,[b] Jin-Xia Yang*[b] and Qipu Lin *[b,c]

a. *College of Chemistry, Fuzhou University, Fuzhou, Fujian 350108, China.*

b. *State Key Laboratory of Structural Chemistry, Fujian Institute of Research on the Structure of Matter, Chinese Academy of Sciences, Fuzhou, Fujian 350002, China.*

c. *Fujian College, University of Chinese Academy of Sciences, Fuzhou, Fujian 350002, China*
E-mail: linqipu@fjirsm.ac.cn

Single Crystal Characterization

Single crystals of the title compounds were carefully selected under an optical microscope and glued onto a thin glass fiber. SCXRD data were collected on a ROD, Synergy Custom system, HyPix diffractometer with Ga Kα (λ = 1.34050 Å) radiation at 100 K or 200 K. All the structures were solved by direct methods and refined on F^2 by full matrix least-squares using Olex2 program.[1] All the non-hydrogen atoms were refined anisotropically. All absorption corrections were performed using the multi-scan program. Crystallographic details are provided in Table S1.

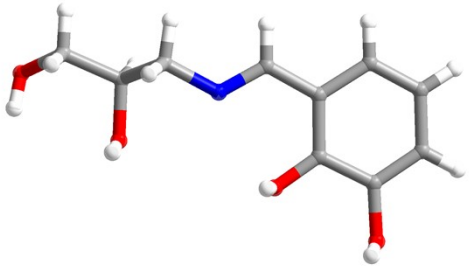

Figure S1. Ball-and-stick representation of the ligand L_1.

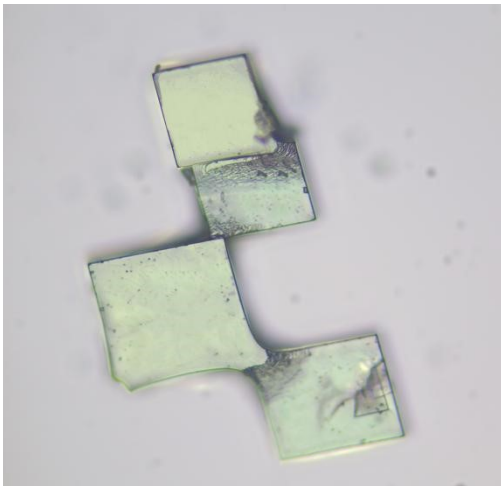

Figure S2. Photograph of as-synthesized D-Sn_4-Boc crystals**.**

Figure S3. Photograph of as-synthesized D-Sn_4-Cbz crystals**.**

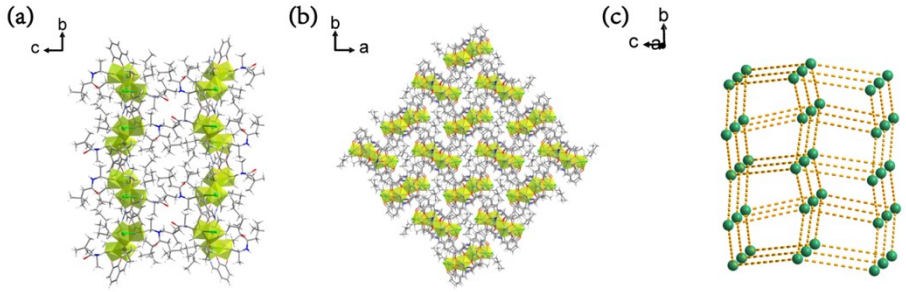

Figure S4. Crystal packing of D-Sn_4-Boc: (a) projection along the a-axis, (b) projection along the c-axis; (c) simplified topological network with each cluster as a node.

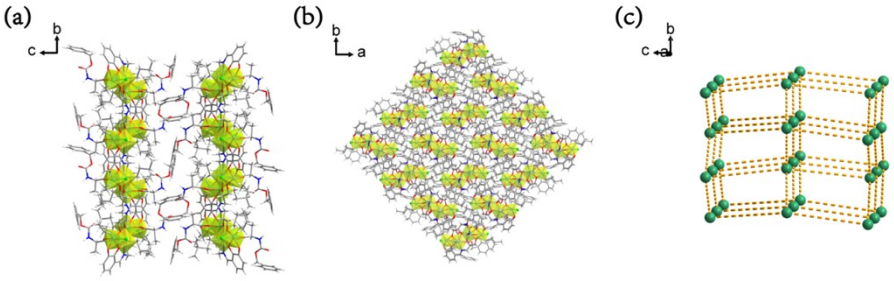

Figure S5. Crystal packing of D-Sn_4-Cbz: (a) projection along the a-axis, (b) projection along the c-axis; (c) simplified topological network with each cluster as a node.

Composite Film Preparation

Composite polymer films were prepared by dispersing the cluster powders into a polyvinylpyrrolidone (PVP) matrix. First, PVP (200 mg) was dissolved in ethanol (3 mL) under stirring to form a clear viscous solution. Then, ground powder of D-Sn_4-Boc or D-Sn_4-Cbz (6×10^{-3} mmol) was added and stirred until a homogeneous yellow dispersion was obtained. A 100 μL aliquot of the dispersion was deposited onto a clean quartz slide (1.5×1.5 cm^2) and spin-coated. After each coating cycle, the films were dried in an oven at 80 ºC. This process was repeated until 10 layers were accumulated, yielding uniform composite films. Pure PVP films were also prepared under identical conditions as blank references. SEM images (Figure S7) reveal smooth and uniform film surfaces, with cross-sectional thicknesses of approximately 2-3 μm for both composite films.

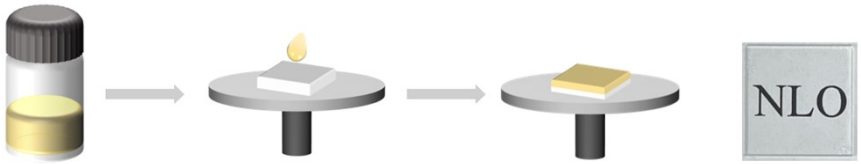

Figure S6. Schematic diagram of composite membranes prepared by incorporating D/L-Sn_4-Boc and D/L-Sn_4-Cbz into a polymer matrix.

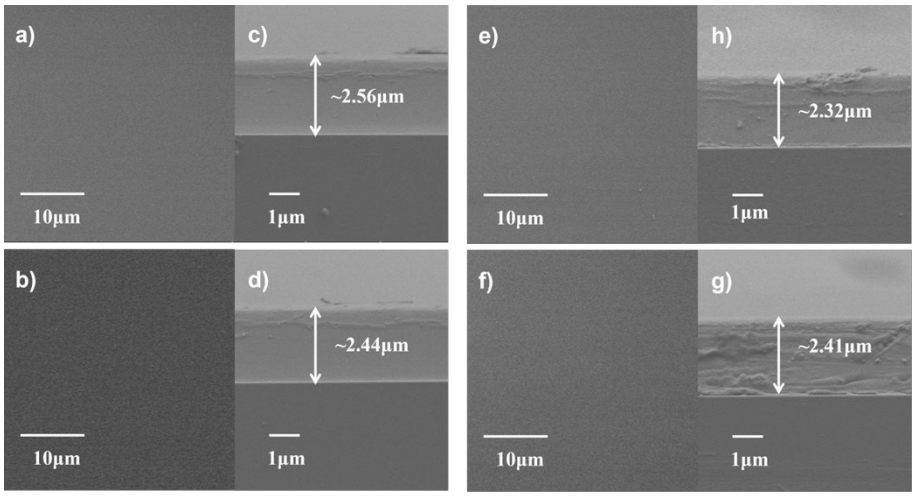

Figure S7. SEM images: (a,b,e,f) surface views of D-Sn_4-Boc@PVP, L-Sn_4-Boc@PVP, D-Sn_4-Cbz@PVP and L-Sn_4-Cbz@PVP films; (c,d,h,g) cross-sectional views of D-Sn_4-Boc@PVP, L-Sn_4-Boc@PVP, D-Sn_4-Cbz@PVP and L-Sn_4-Cbz@PVP films.

Nonlinear Optical Measurements

Third-order nonlinear optical (NLO) properties were evaluated using the open-aperture (OA) *Z*-scan technique. The experimental setup employed a Nd:YAG laser (532 nm, 10 Hz repetition frequency) as the excitation source. Samples were mounted on a program-controlled rail that allowed for movement along the *z*-axis. Transmitted energy was recorded by two detectors (D1, D2) placed before and after the sample. The transmittance values of D-Sn_4-Boc@PVP and D-Sn_4-Cbz@PVP films were measured to be 0.72 and 0.84, respectively. All measurements were conducted at room temperature.

The normalized transmittance $T(Z, S = 1)$ for an open-aperture configuration is given by:

$$T(Z, S = 1) = \frac{1}{\sqrt{\pi} q_0(Z,0)} \int_{-\infty}^{\infty} \ln\left[1 + q_0(Z,0) e^{-r^2}\right] dr$$

where

$q_0(Z,0) = \beta I_0 L_{eff}$

$L_{eff} = [1 - exp(-\alpha l)]/\alpha$

Here, I_0 represents the on-axis peak intensity at the focus ($Z = 0$), L_{eff} is the effective thickness of the sample, l is the actual sample thickness, and a is the linear absorption coefficient. The nonlinear absorption coefficient β was determined by fitting the experimental transmittance data.

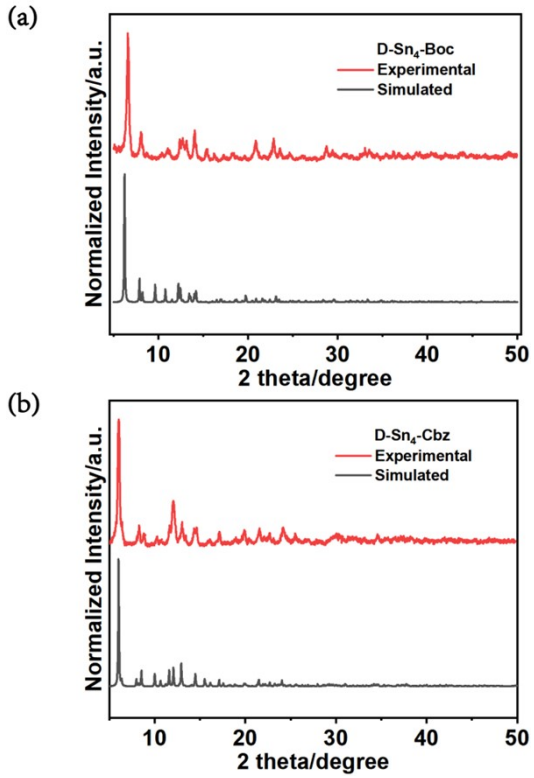

Figure S8. Simulated and experimental PXRD patterns of D-Sn_4-Boc and D-Sn_4-Cbz. Minor intensity variations between simulated and experimental patterns are attributed to preferential crystal orientation effects.[2]

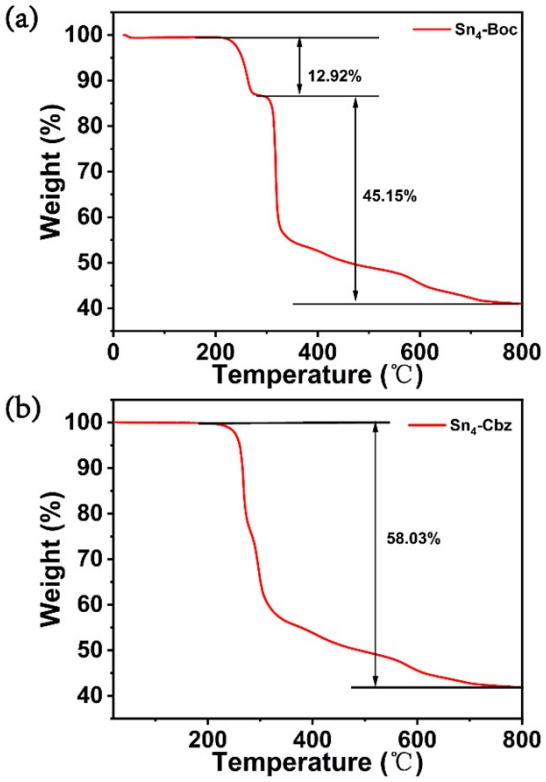

Figure S9. TGA curves of D-Sn_4-Boc and D-Sn_4-Cbz under N_2 atmosphere.

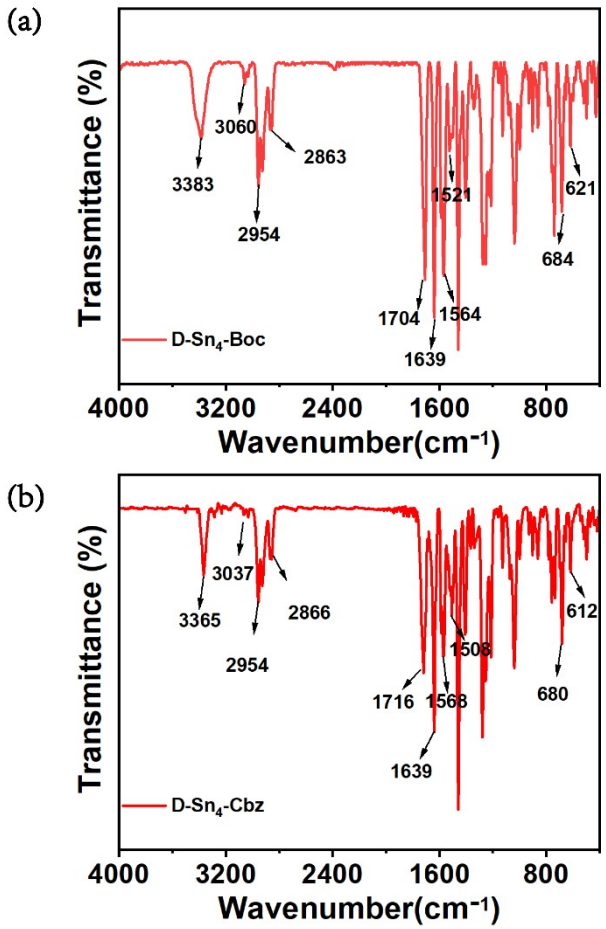

Figure S10. FT-IR spectra of D-Sn_4-Boc and D-Sn_4-Cbz (KBr pellets, 400 – 4000 cm^{-1}).

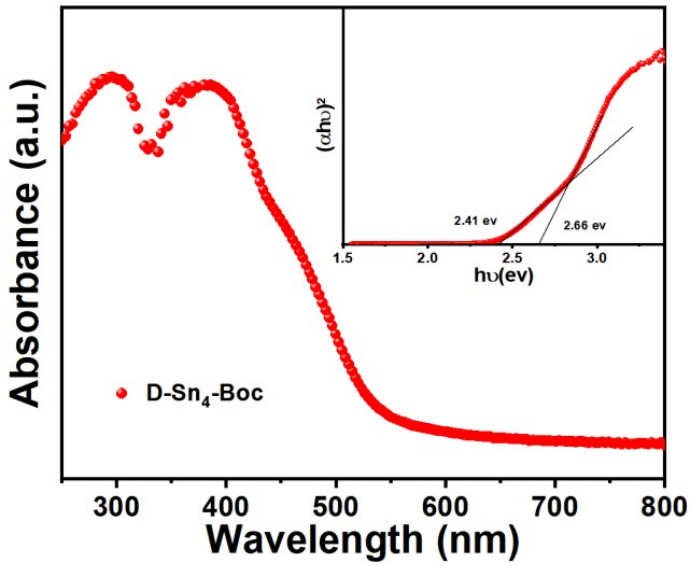

Figure S11. Solid-state UV-Vis absorption spectrum and Tauc plot of D-Sn_4-Boc.

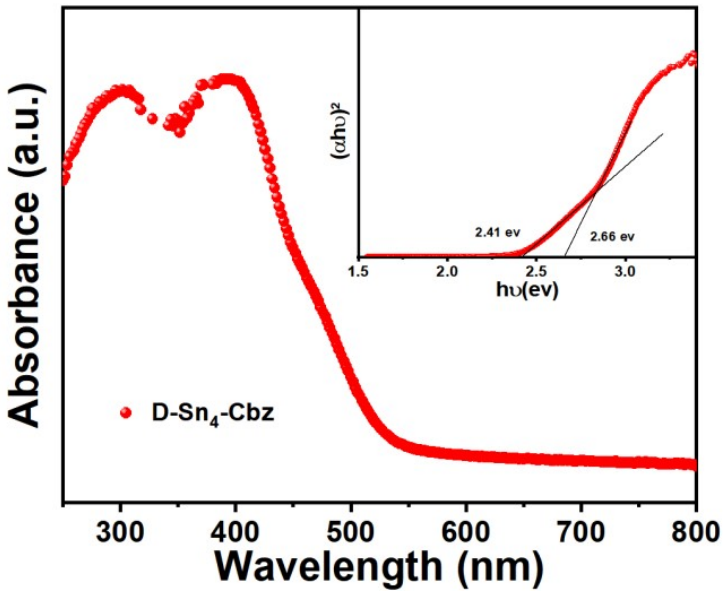

Figure S12. Solid-state UV-Vis absorption spectrum and Tauc plot of D-Sn_4-Cbz.

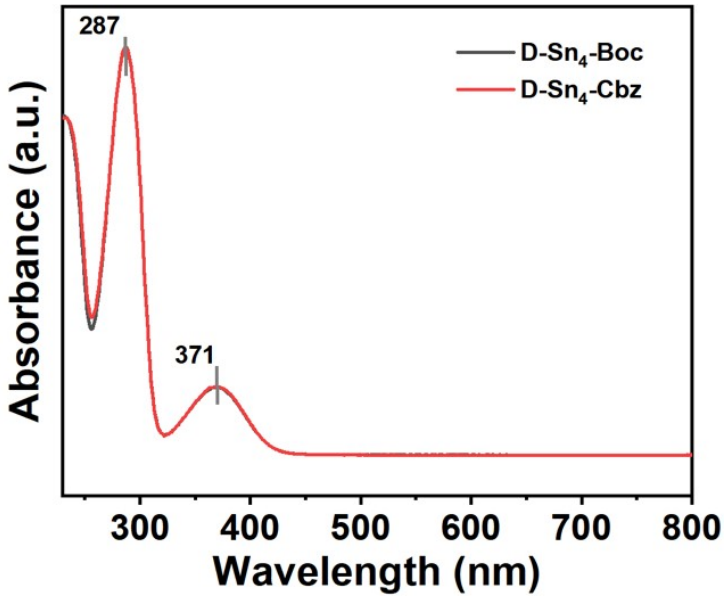

Figure S13. UV-Vis absorption spectra of D-Sn_4-Boc and D-Sn_4-Cbz in MeCN.

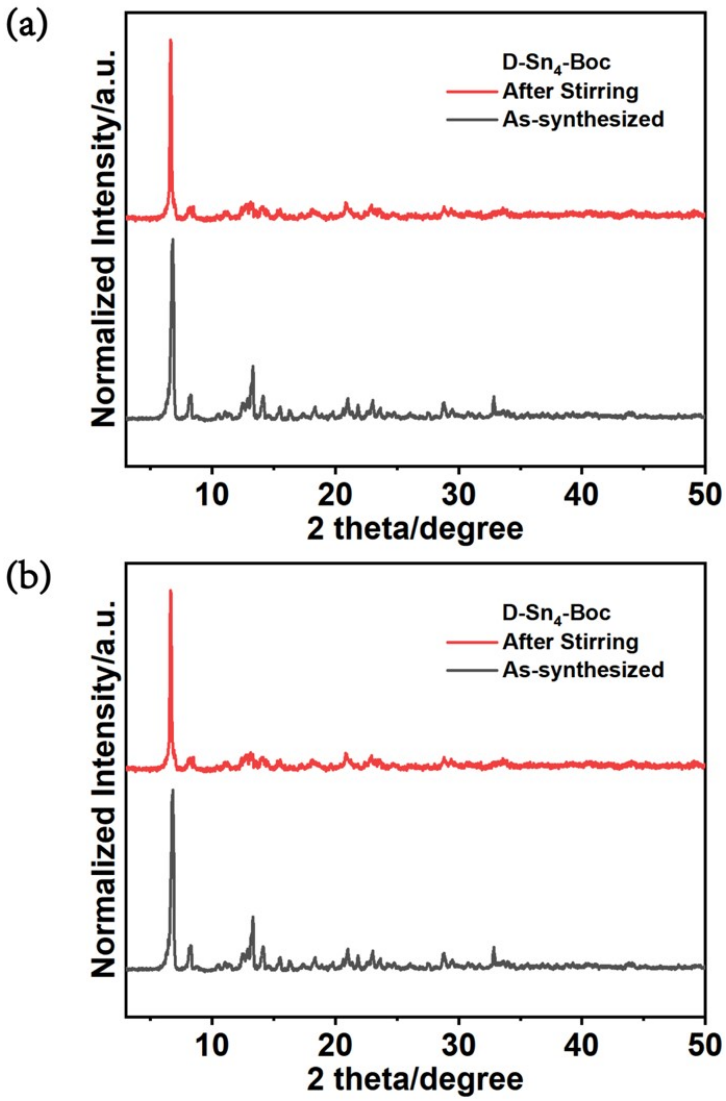

Figure S14. PXRD patterns of D-Sn_4-Boc and D-Sn_4-Cbz before and after stirring in a PVP/ethanol solution for 24 h.

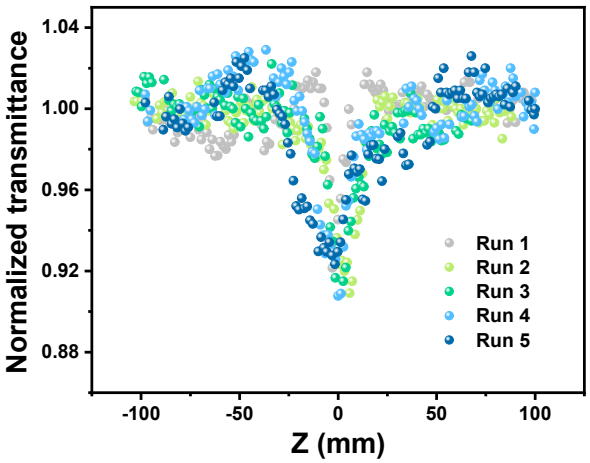

Figure S15. Reproducibility test: open-aperture Z-scan curves measured at five

different positions on the same D-Sn_4-Boc@PVP film.

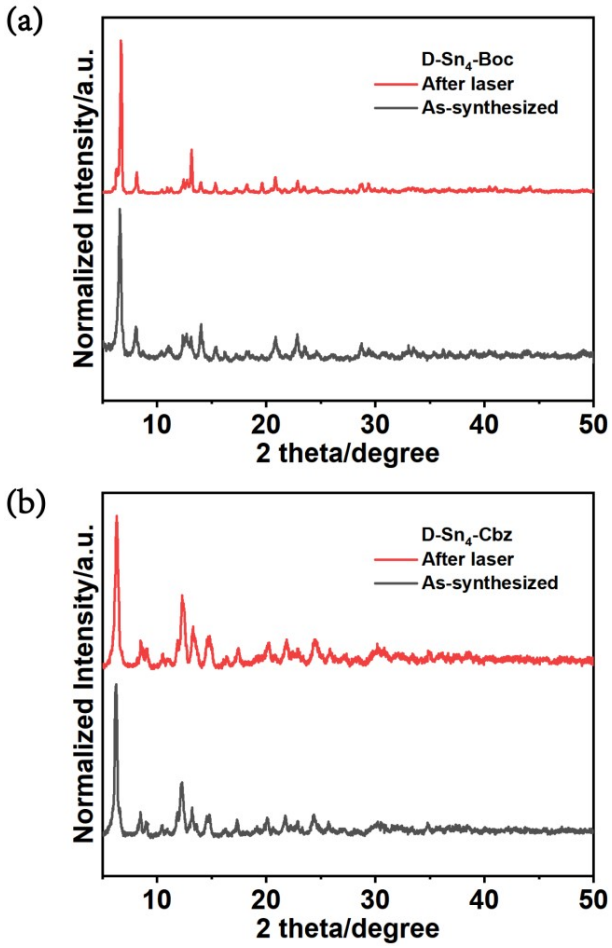

Figure S16. PXRD of D-Sn_4-Boc and D-Sn_4-Cbz crystal before and after continuous 532 nm laser irradiation for 3 h.

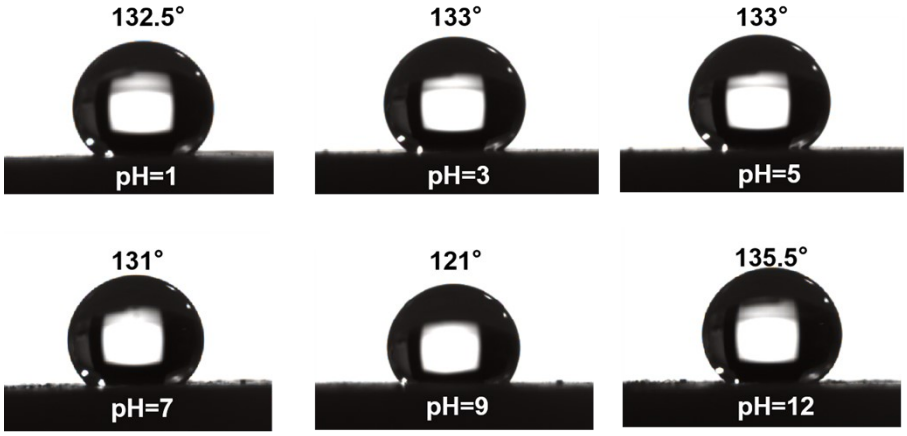

Figure S17. Water contact-angle photographs of D-Sn_4-Boc after 7-day immersion in aqueous solutions of pH 1-12.

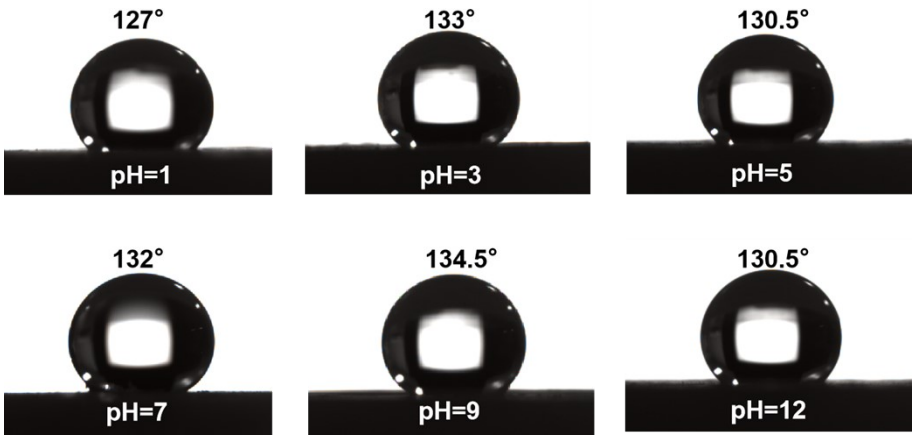

Figure S18. Water contact-angle photographs of D-Sn_4-Cbz after 7-day immersion in aqueous solutions of pH 1-12.

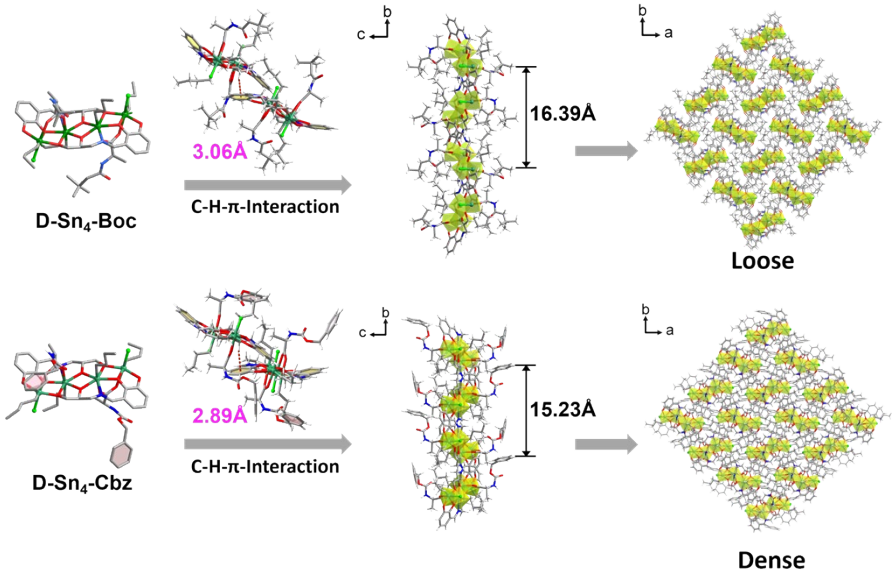

Figure S19. Supramolecular packing diagrams illustrating the helical arrangement of clusters along the a- and c-axes for D-Sn_4-Boc and D-Sn_4-Cbz.

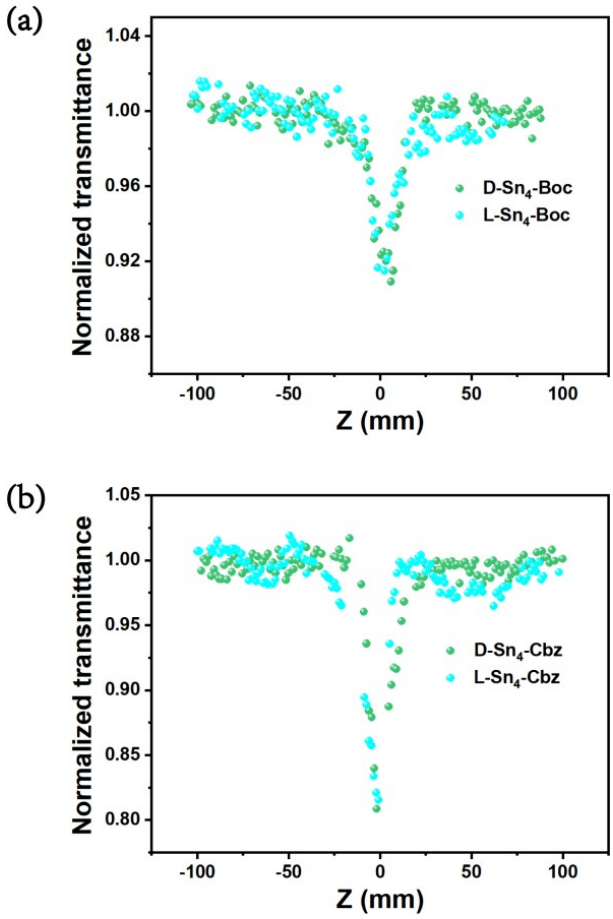

Figure S20. Open-aperture Z-scan diagrams for D/L-enantiomers of Sn_4-Boc@PVP and Sn_4-Cbz@PVP films at 532 nm.

Table S1 Crystallographic data and refinement parameters for D/L-Sn_4-Boc and D/L-Sn_4-Cbz

Parameter	D-Sn_4-Boc	L-Sn_4-Boc
Formula	$C_{54}H_{86}Cl_2N_4O_{14}Sn_4$	$C_{54}H_{86}Cl_2N_4O_{14}Sn_4$
Fw	1560.92	1560.92
Space group	$P2_12_12_1$	$P2_12_12_1$
a (Å)	15.1734(2)	15.1563(2)
b (Å)	16.3910(2)	16.4024(2)
c (Å)	27.2785(4)	27.3019(3)
α (°)	90	90
β (°)	90	90
γ (°)	90	90
V (Å^3)	6784.36(16)	6787.24(14)
Z	4	4
D_{calcd} (g cm^{-3})	1.528	1.528
Temp (K)	200.00(10)	200.00(10)
μ (mm^{-1})	8.713	8.710
F (000)	3136.0	3136.0
Reflections collected	77159	75276
GOF	1.081	1.063
[a]R_1, wR_2 ($I > 2\sigma(I)$)	0.0503/ 0.1365	0.0544/0.1563
[b]$R1$, wR_2 (all data)	0.0554/ 0.1401	0.0606/0.1613
CCDC number	2522100	2522701

[a]$R_1 = \sum ||F_o| - |F_o|| / \sum |F_o|$. [b]$wR_2 = [\sum w(F_o^2 - F_c^2)^2 / \sum w(F_o^2)^2]^{1/2}$.

Parameter	D-Sn_4-Cbz	L-Sn_4-Cbz
Chemical formula	$C_{58}H_{78}Cl_2N_4O_{16}Sn_4$	$C_{58}H_{78}Cl_2N_4O_{16}Sn_4$
Fw	1632.86	1632.90
Space group	$P2_12_12_1$	$P2_12_12_1$
a (Å)	15.0434(2)	15.0620(4)
b (Å)	15.2331(3)	15.1736(6)
c (Å)	29.7454(7)	29.6663(15)
α (°)	90	90
β (°)	90	90
γ (°)	90	90
V (Å^3)	6816.4(2)	6780.1(5)
Z	4	4
D_{calcd} (g cm^{-3})	1.591	1.600
Temp (K)	99.99(14)	100.00(10)
μ (mm^{-1})	8.759	8.755
F (000)	3264.0	3264.0
Reflections collected	67027	71436
GOF	1.019	1.008
[a]R_1, wR_2 ($I > 2\sigma(I)$)	0.0865/0.2197	0.1162/0.3172
[b]$R1$, wR_2 (all data)	0.1069/0.2353	0.1386/0.3397
CCDC number	2522101	2522700

[a]$R_1 = \sum ||F_o| - |F_o|| / \sum |F_o|$. [b]$wR_2 = [\sum w(F_o^2 - F_c^2)^2 / \sum w(F_o^2)^2]^{1/2}$.

References

1. G. Sheldrick, SHELXT-Integrated Space-Group and Crystal-Structure Determination, *Acta Cryst. A*, 2015, **71**, 3-8.
2. L. Zhang, A. A. S. Gonçalves and M. Jaroniec, Identification of Preferentially Exposed Crystal Facets by X-ray Diffraction, *RSC Adv.*, 2020, **10**, 5585-5589.